

# Porous phosphate heterostructures containing CdS quantum dots: assembly, characterization and photoluminescence

Manuel Algarra · Iulius Bobos · José Jiménez-Jiménez ·  
Ramón Moreno-Tost · Enrique Rodríguez-Castellón ·  
Joaquim C. G. Esteves da Silva

Received: 21 July 2009 / Accepted: 9 November 2009 / Published online: 22 November 2009  
© Springer Science+Business Media B.V. 2009

**Abstract** The synthesis and characterization of cadmium sulphide (CdS) quantum dots, conjugated in a porous phosphate heterostructure functionalized with aminopropyl groups is described. The resulting material has fluorescence properties with maximum emission intensity at 575 nm. The fluorescent materials are not soluble in water and exhibit high stability in aqueous solution in the pH ranges from 2 to 9. Energy dispersive X-ray spectroscopy confirmed the qualitative elemental composition of the synthesized materials and X-ray photoelectron spectra showed a surface S/Cd atomic ratio of 1.09. SEM images show that the materials are amorphous, possessing porous with sizes of several tens nanometres, homogeneous and exhibit a layered morphology. The adsorption–desorption analysis by N<sub>2</sub> at 77 K showed the accessibility of the CdS quantum dots onto the pores of the structure. The CdS quantum dots were stabilized by mercaptopropionic acid and bounded to the host materials by amine groups.

Presented in the NANO Conference 2009 April 5–7, Riyadh, Saudi Arabia.

M. Algarra (✉) · I. Bobos  
Centro de Geologia do Porto, Faculdade de Ciências,  
Universidade do Porto, Rua do Campo Alegre 687,  
4169-007 Porto, Portugal  
e-mail: magonzal@fc.up.pt

J. Jiménez-Jiménez · R. Moreno-Tost · E. Rodríguez-Castellón  
Departamento de Química Inorgánica, Facultad de Ciencias,  
Universidad de Málaga, Campus de Teatinos s/n,  
29071 Málaga, Spain

J. C. G. Esteves da Silva  
Centro de Investigação em Química (CIQ-UP), Faculdade  
de Ciências da Universidade do Porto, Rua do Campo Alegre  
687, 4169-007 Porto, Portugal

**Keywords** Functionalized phosphate heterostructure · CdS quantum dots · Luminescent materials

## Introduction

Modern material science devotes particular attention to studies of new materials for a wide range of applications. Nowadays an area of interest is closely related to the development of highly luminescent quantum dots (QDs), nanoparticles with semiconductor character which posses unique electronic properties and great analytical chemical potential [1–4]. Moreover, it is a focus of interest the development of assemblies of QDs into appropriate confinement to enhance their stability and luminescent and create nanostructural materials with unique physical and chemical properties [5, 6]. Moreover, nanoparticles aggregation is a problem [7] that can be minimized by their encapsulation in a chemically inert matrix also, this allow an accurately control dispersion of the nanoparticles. The extension of the dispersion of nanoparticles on a solid material depends on the uniformity of the pores of the matrix. Matrices with uniform pore structure and controlled diameter are preferable as host materials for nanoparticles.

The nanolevel uniform pore structures of mesoporous materials, such porous phosphate heterostructure (PPH) [8], seems a challenge system to build nanocomposites systems, owing to the possibility to obtain materials with different pore size (2–50 nm) and structures. Mesoporous materials are being developed as a very promising and aesthetically appealing area of chemistry since the disclosure of the MCM 41 family, in the earliest nineties [9, 10].

PPH are being proposed due to the new strategies of synthesis, are the latter template obtained by using

zirconium phosphate as a layered structure which is expanded with cationic surfactants in order to form silica galleries in the interlayer space, by coupling synthetic methodologies used for producing pillared layered structures and mesoporous solids such as the MCM 41 family. A porous material with a high specific surface area is obtained when the surfactant molecule, used as template is removed. The presence of this porous distribution confers these materials excellent potential host properties for nanoparticles, as QDs [11]. Moreover, PPH are materials that can be easily functionalised allowing an increased affinity towards selected substances and nanoparticles. For example, to facilitate the transport of nanoparticles precursor molecules or ions inside the channels of mesoporous materials, it is proposed the use of functional ligands randomly distributed through the internal surface of PPH [12]. Recently, PPH have been successfully investigated as supported of copper [13] and ruthenium [14] in catalyst process.

In this work, a simple and flexible method for the direct synthesis of a conjugated N-PPH-CdS is presented. The CdS are formed in the functionalized hybrid PPH structure. The CdS is a very attractive semiconductor material due to its stability, photochemical properties and easy preparation and handling as well as the practical applications in photonics and electronics [15] or analytical purposes [16–18]. Because the novelty of these synthesised materials and their wide applications, functionalized PPH are used as host materials for CdS QDs nanoparticles to obtain their spectroscopy behaviour in such as matrix.

## Materials and methods

### Synthesis of PPH host and functionalized N-PPH

The synthesis of the host PPH and the PPH functionalized with amine groups (N-PPH) were synthesised according the previous published bibliography [8, 19]. In this work, was chosen a molar ratio of 5 and 50 in tetraethylorthosilicate (TEOS) and the corresponding aminopropyl triethoxysilane (APTEOS).

### Synthesis of N-PPH-CdS QDs conjugated material

N-PPH (6.2 mg) was suspended in 1-propanol and stirred for 4 h at room temperature, excess of cadmium chloride ( $\text{CdCl}_2$ ) was added (7.5 mg) and left to stabilize for 24 h in order to allow the coordination of  $\text{Cd}^{2+}$  by the amine groups of N-PPH. Gently, 100  $\mu\text{L}$  (1.14 mmol) of 3-mercaptopropionic acid (MPA) was added and left to stabilize during 4 h, equimolar sodium sulfide ( $\text{Na}_2\text{S}$ ),  $9.07 \times 10^{-6}$  moles, was added to obtain a turbid yellowish solution; its centrifugation allowed the separation of brightness yellowish solid. This solid was washed twice with ethylic ether to remove the 1-propanol residues and left to evaporate in vacuum. The purification of the N-PPH-CdS was done by dialyzes for 48 h against deionised water using a MW CO 12,000–14,000 Da dialysis tube from Medicell International. The density of aminopropyl groups and the textural parameters of these materials used as host for QDs are presented in the Table 1. As expected when the density of aminopropyl groups increases, the surface area and volume of pores of the materials decreases.

The  $\text{CdCl}_2$  and  $\text{Na}_2\text{S}$  were added into the 1-propanol suspension containing N-PPH,  $\text{Cd}^{2+}$  was absorbed onto the surface of the PPH by both electrostatic and coordination interactions between  $\text{Cd}^{2+}$  and the aminopropyl groups on N-PPH [20], and  $\text{S}^{2-}$  bounded to  $\text{Cd}^{2+}$  originating CdS QDs. Also, nanoparticles of CdS of highest size can be formed onto the surface of N-PPH host, where also aminopropyl groups are presented. After purification a bright yellowish powder was obtained. Figure 1a shows a photograph of grains of N-PPH-CdS dispersed in a buffer solution excited at 401 nm, the Fig. 1b shows the corresponding emission spectra.

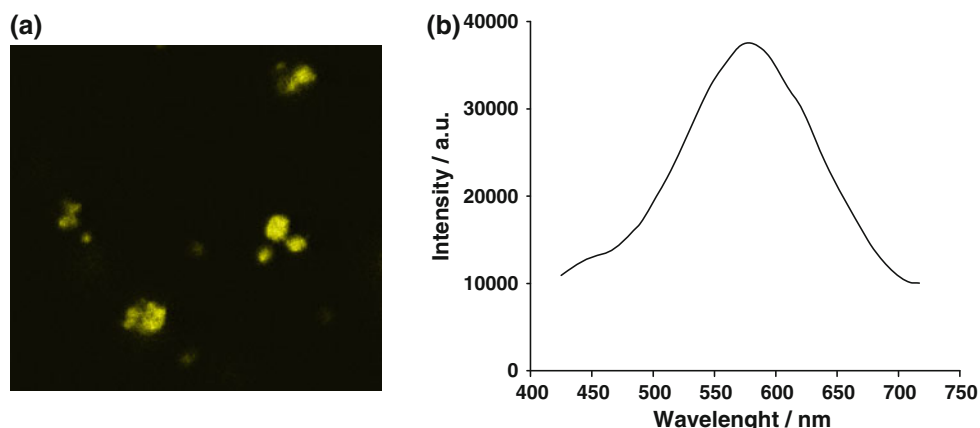
The fluorescence properties of the material were analysed by dispersing grains in different pH buffer solutions, in the range 2–9, and any variation of the emission maximum was observed. Also, the material did not dissolve or decompose in these aqueous buffer solutions for several days. The maximum of the emission spectra at all pH values was  $576 \pm 3$  nm (average and standard deviation). It is suggested that the N-PPH structure confer a protection to thus luminescent system.

**Table 1** Textural parameters of N-PPH materials before and after conjugation with QDs

Material	N-PPH host			N-PPH-CdS	
	Aminopropyl groups (mmol/100 g)	$S_{\text{BET}}$ ( $\text{m}^2 \text{ g}^{-1}$ )	$V_p$ ( $\text{cm}^3 \text{ g}^{-1}$ )	$S_{\text{BET}}$ ( $\text{m}^2 \text{ g}^{-1}$ )	$V_p$ ( $\text{cm}^3 \text{ g}^{-1}$ )
$\text{N}_5\text{-PPH-CdS}$	127	223	0.411	41	0.219
$\text{N}_{50}\text{-PPH-CdS}$	20	556	0.618	186	0.502

$S_{\text{BET}}$ , surface area per gram of material calculated using BET method;  $V_p$ , volume of pores per gram of material calculated using BJH method

**Fig. 1** **a** Luminescence image of N-PPh-CdS grains (excitation at 401 nm) and **b** the corresponding emission spectra



This maximum emission wavelength fall in the range observed for CdS QDs literature values for the maximum emission wavelength for CdS QDs are: L-cysteine-capped-CdS, 495 nm [18], L-cysteine-capped-CdS, thioglycerol-capped-CdS and polyphosphate-capped-CdS, 460, 560 and 650 nm, respectively [16], mercaptoacetic acid-capped-CdS, 541 nm [17].

#### Characterization methods

Scanning Electron Microscopy (SEM) and energy-dispersive X-ray spectroscopy (EDS) of the purified material were carried out on a FEI Quanta 400FEG/EDAX Genesis X4M High Resolution Scanning Electronic Microscope, the sampling accessory was 400 mesh copper/carbon grids (Electron Microscopy Sciences, Hatfield, PA, USA) attached to a steel support. Transmission Electron Microscopy (TEM) was carried out with a Philips CM-200.

Confocal microscope images were acquired with a Leica SP2 AOBS SE (Leica Microsystems, Germany) using solid N-PPh-CdS dispersed in 0.1 M phosphate buffer solutions in the pH range between 2 and 9.

X-ray photoelectron spectra (XPS) were obtained using a Physical Electronics PHI 5700 spectrometer with a non-monochromatic Al K $\alpha$  radiation (300 W, 15 kV,  $h\nu = 1486.6$  eV) as the excitation source. Spectra were recorded at 45° take-off angle by a concentric hemispherical analyser operating in the constant pass energy mode at 25.9 eV, using a 720  $\mu\text{m}$  diameter analysis area. Under these conditions the Au 4f<sub>7/2</sub> line was recorded with 1.16 eV FWHM at a binding energy of 84.0 eV. The spectrometer energy scale was calibrated using Cu 2p<sub>3/2</sub>, Ag 3d<sub>5/2</sub> and Au 4f<sub>7/2</sub> photoelectron lines at 932.7, 368.3 and 84.0 eV, respectively. Charge referencing was done against adventitious hydrocarbon (C 1s 284.8 eV). Powdered solids were mounted on a sample holder without adhesive tape and kept overnight in high vacuum in the preparation chamber before they were

transferred to the analysis chamber of the spectrometer. Each region was scanned with several sweeps until a good signal to noise ratio was observed. The pressure in the analysis chamber was maintained lower than  $10^{-9}$  Torr. A PHI ACCESS ESCA-V6.0 F software package was used for acquisition and data analysis. A Shirley-type background was subtracted from the signals. Recorded spectra were always fitted using Gauss–Lorentz curves in order to determinate more accurately the binding energy of the different element core levels. The accuracy of binding energy's (BE's) values was within  $\pm 0.1$  eV.

FTIR spectra were recorded in the 4,000–400  $\text{cm}^{-1}$  frequency region using a Brucker Tensor-27 IR-spectrophotometer equipped with a room temperature DTGC-detector. The measurements of the absorption bands integrated intensity were made using the OPUS software supplied by the Brucker Instrument. The pellet discs of 0.8 cm diameter were prepared by mixing 1 mg sample with 200 mg KBr and pressing at 14  $\text{kg}/\text{cm}^2$ . Prior to analysis, the pellets were overnight heated at 80 °C to remove any adsorbed water.

X-ray diffraction (XRD) spectroscopy patterns of powdered specimens were obtained using a Rigaku Miniflex D/max-C series automated diffraction system equipped with a graphite monochromator and a Cu K $\alpha$  radiation. Samples were analyzed in the range 4–70° $2\theta$ , using a 1° divergence slit, a step increment of 0.05° $2\theta$  and a counting time of 5 s/step.

Textural parameters were obtained from  $\text{N}_2$  adsorption–desorption isotherms (BET method) with a Micromeritics ASAP 2020. The specific surface area and pore volume of the CdS-NPPH were determined by the adsorption–desorption of  $\text{N}_2$  at –196 °C with a Micromeritics ASAP 2020. The specific surface area of N-PPh-CdS in a dry state was determined by multipoint Brunauer–Emmett–Teller (BET) method. Before analysis, the N-PPh-CdS sample was degassed at 150 °C up to  $10^{-4}$  Torr. Pore

volume and an average pore diameter for N-PPH-CdS were determined by the Barrett, Joyner, Halenda model.

## Results and discussion

### EDS and XPS analysis

EDS qualitative measurements were performed on the N-PPH-CdS and the corresponding spectrum is shown in Fig. 2. This spectrum shows strong signals of Cd and S from the CdS QDs, and Zr, P, N and O from N-PPH-CdS (the signals of Cu, Al and C are due to the SEM grids). These EDS results confirm the presence of CdS QDs conjugated with N-PPH.

The XPS, in terms of surface composition, showed a surface S/Cd atomic ratio is 1.09, near to the theoretical S/Cd atomic ratio value for bulk CdS (1.00). This is indicative of a homogeneous distribution of the CdS nanoparticles on the external surface. The core level S 2p and Cd 3d spectra are shown in Fig. 3. The S 2p<sub>3/2</sub> peak appears at 162.1 eV, slightly higher than the value reported in the literature for pure CdS (161.7 eV) [21] and can be attributed to the interaction of amino groups from N-PPH with CdS. While the Cd 3d<sub>5/2</sub> peak appears at 405.4 eV, similar to the value observed for pure CdS [22]. These data confirm the presence of CdS on the surface of the solids.

### SEM and TEM images

A typical SEM image of the material is shown in Fig. 4. The analysis of this figure confirm that the material is amorphous possessing porous with sizes of several tens nanometres, is homogeneous and present a layered morphology. The size distributions of CdS QDs synthesized

**Fig. 2** EDS spectra of N-PPH-CdS

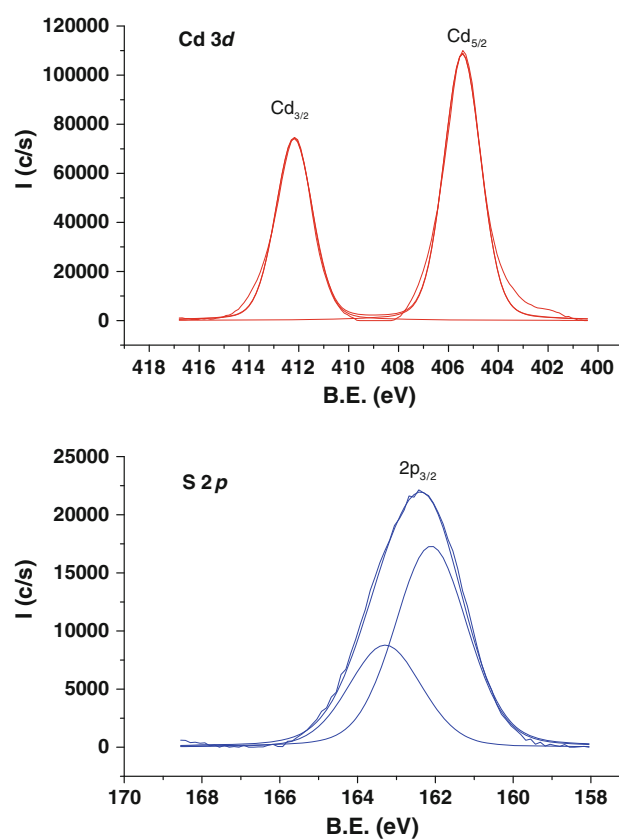
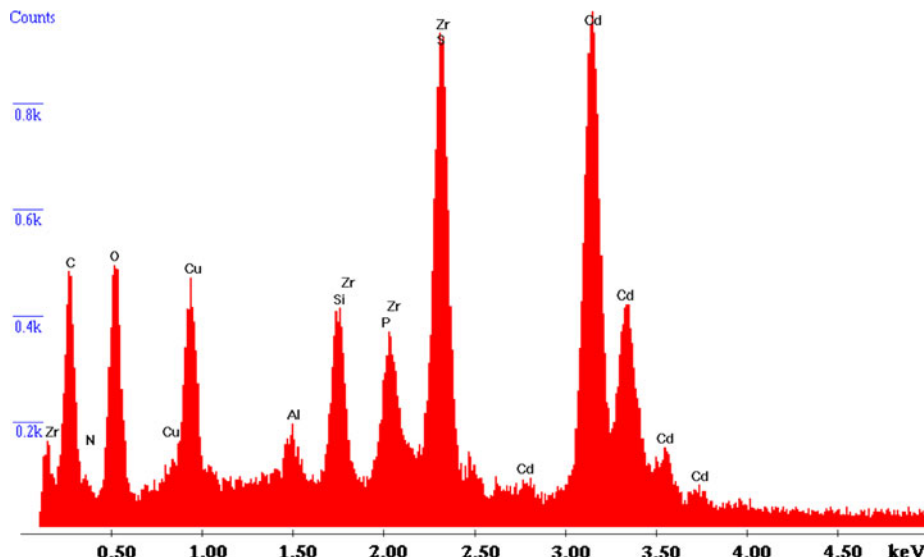


**Fig. 3** **a** Cd 3d and **b** S 2p core level spectra of CdS in the N-PPH materials

inside N-PPH are comprised between 20 and 40 nm. While for the CdS nanocrystals, due to the hardness for controlling their surface situation, in most cases, the visible emission around orange region arise from the recombination of CdS nanocrystal surface trap states is inevitably observed, and their bandgap emission at blue region is

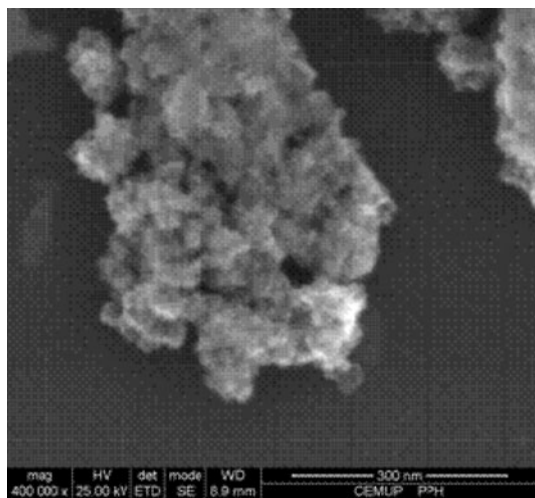


**Fig. 4** SEM photograph of N-PPH-CdS

hardly realized because of the trap states abundant on the nanocrystal surfaces. Therefore, by changing the surface situation, it is possible to leverage the band-edge emission and surface trap state emission of CdS nanocrystals to achieve orange luminescence. TEM image (Fig. 5a) shows the CdS nanoparticles (see dark bits) which are occluding the pores of pristine NH-PPH materials. The measurement size of the CdS nanoparticles is about 1–3 nm. Also, aggregates of CdS and pristine are shown in Fig. 5b. The chemical elements distribution along a horizontal profile at about 800 nm in length using energy dispersive X-ray spectroscopy analysis show to the left part of the profile line a composition constituted by S and Cd, whereas the

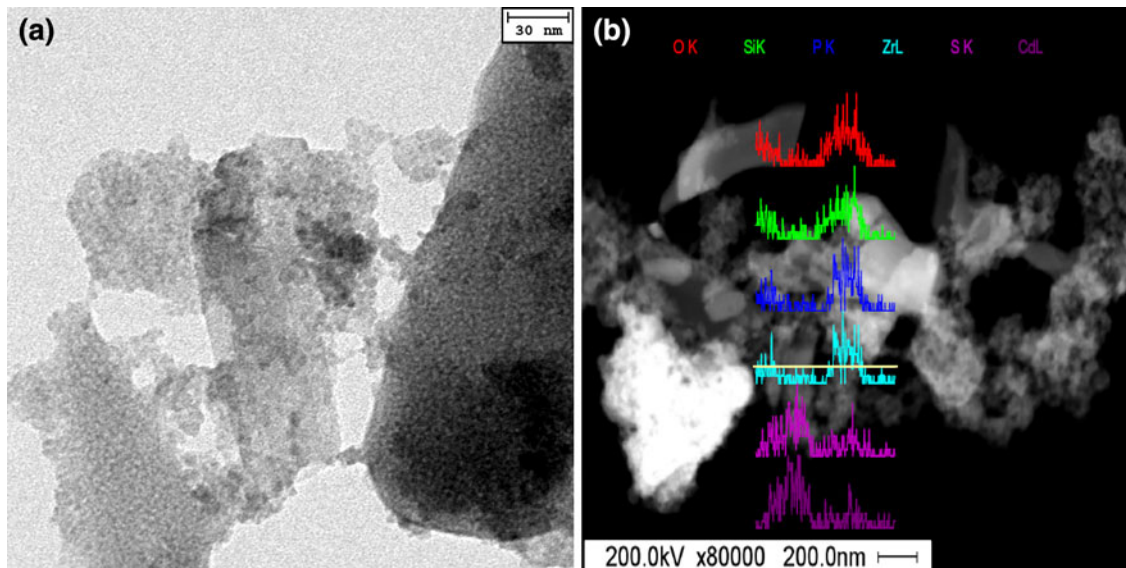
particles located to the right part have a chemical composition (O, Si, P and Zr) corresponding to N-PPH material.

#### FT-IR analysis

The FT-IR spectrum of the host materials suffers marked modifications when conjugated, example for N-PPH in Fig. 6. Host materials exhibit a band at  $1,640\text{ cm}^{-1}$ , characteristic of primary amines. This band suffers a shift and apparent intensity attenuation when the material is conjugated, suggesting that the amine groups of N-PPH participate in the binding to CdS QDs. The broad band with a maximum at  $1,080\text{ cm}^{-1}$  is the overlapped of several stretching bands, for example, P–O and C–N. The conjugated materials show a strong band at  $1,700\text{ cm}^{-1}$ , not detected in the host materials, which is due to the stretching of the carbonyl groups of MPA. These results show that CdS QDs are stabilized by MPA and bounded to the host materials by amine groups.

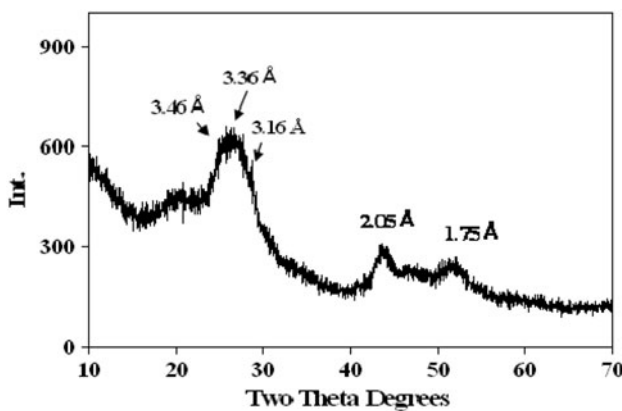
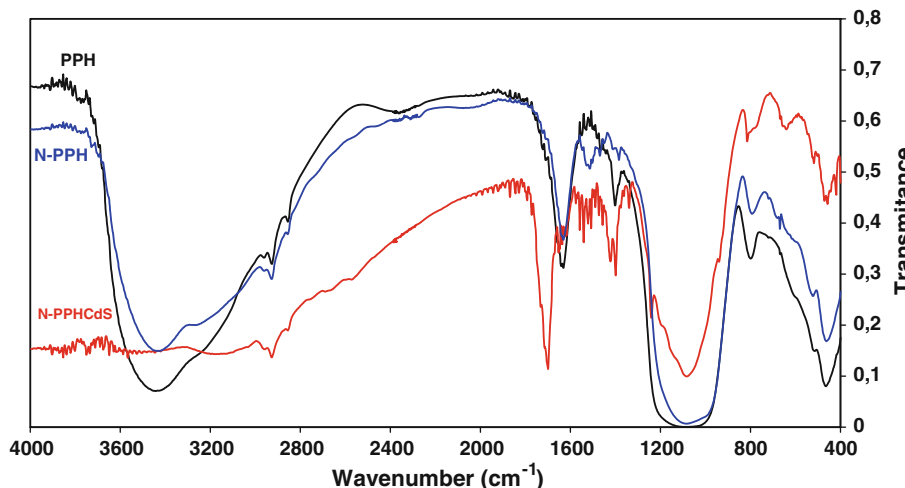
#### XRD

Figure 7 shows the XRD pattern of N-PPH-CdS. The XRD of hosts N-PPH showed, as expected, an amorphous structure, due to that the silica structure of galleries is non-crystalline. The powder XRD patterns is characterised by a broad peak with a mean value occurring at about  $3.36\text{ \AA}$  ( $26.51, 2\theta$ ), corresponding to the d(111) diffraction plane of  $\beta$ -CdS (Hawleyite) by comparison with data from JCPDS file no. 10-454. Also, two more bands, at  $2.06\text{ \AA}$  ( $43.9, 2\theta$ ) and  $1.75\text{ \AA}$  ( $52.0, 2\theta$ ) corresponding to d(220) and d(311) diffraction



**Fig. 5** **a** TEM images of CdS nanoparticles (dark bits) confined in the pristine N-PPH. **b** EDS spectra obtained on the CdS and pristine aggregates

**Fig. 6** FT-IR spectra of N-PPH and N-PPH-CdS



**Fig. 7** XRD patterns of randomly powdered oriented samples of N-PPH-CdS

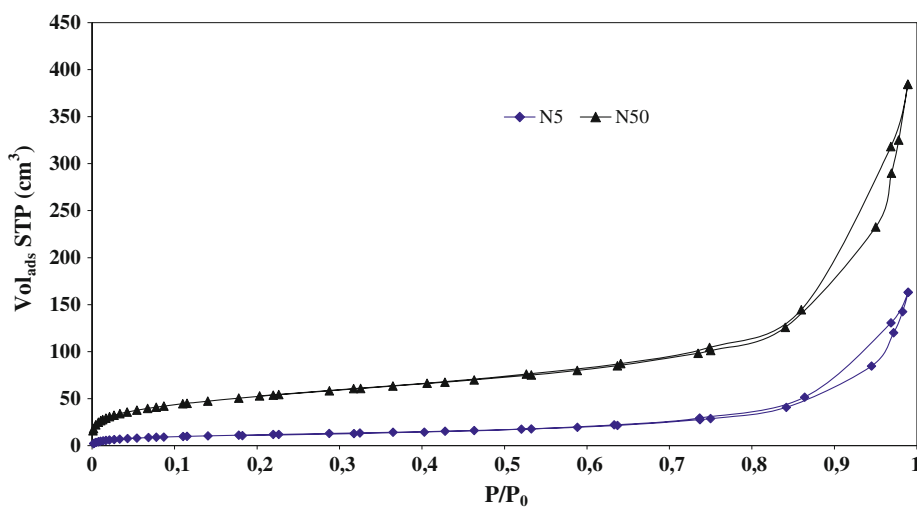
planes, are associated with  $\beta$ -CdS (cubic system, F43M) [JCPDS file, no. 10-454], [23]. The broadness of the d(111) peak could be related to the smaller size of the CdS nanoparticles, where the mean size estimated from the Scherrer's

equation is about 3.4 nm [23]. Nevertheless, two other peaks are observed at 3.53 and 3.15  $\text{\AA}$  after the d(111) peak decomposition, that could correspond to the d(100) and d(101) diffraction planes of  $\alpha$ -CdS (Greenockite) [JCPDS file, no. 6-314]. Both peaks and the peak at 3.36  $\text{\AA}$  corresponding to d(002) plane could be also associated with a hexagonal form of CdS (P63mc) [JCPDS file, no 6-314]. Evidences of the d(100) and d(101) planes were observed several published works [23, 24]. Therefore, the band broadening should be caused by a mixture constituted by both hexagonal and cubic forms of  $\beta$ -CdS and  $\alpha$ -CdS. As the time reaction run increases, the d(002) plane become sharper, meaning that a possible transformation from  $\alpha$ -CdS to  $\beta$ -CdS could occur. The broad band peaks are characteristic of CdS QDs and an indication the nano-dimensions of the samples [25].

#### Textural properties of N-PPH-CdS

The surface area of the QDs conjugated materials were evaluated by the BET method the corresponding results are

**Fig. 8** Adsorption–desorption isotherms of  $\text{N}_2$  at 77 K of N5 (filled diamond) and N50 (filled triangle)



compiled in Table 1 and the adsorption–desorption isotherms shown in Fig. 8. The surface area values ( $S_{\text{BET}}$ ) of the host materials suffer a marked decrease when conjugated with QDs, being more marked for the N<sub>50</sub>-PPH-CdS sample (82% reduction) which had more available amino groups to coordinate CdS particles. For the other two materials the reduction in the  $S_{\text{BET}}$  was 67% (N<sub>5</sub>-PPH). This marked decrease in the  $S_{\text{BET}}$  point out that CdS QDs are formed inside the galleries of the host materials, provoking a blockage of the mesopores, impeding the filling of the pores by N<sub>2</sub>. In opposition to the samples N<sub>5</sub>-PPH-CdS and N<sub>50</sub>-PPH-CdS, which show the expected volumes of pores reduction upon conjugation.

## Conclusions

CdS QDs were successfully conjugated with N-PPH via complexation at room temperature under ambient pressure. Well-dispersed CdS QDs were bounded to the mesoporous nanostructure of the N-PPH. CdS QDs were stabilized by MPA and bounded to the host materials by amine groups. The conjugated materials were fluorescent and their photophysical properties were independent of the pH of the aqueous solution in the range of pH between 2 and 9. Also, the conjugated materials were mechanically stable in aqueous solution.

**Acknowledgments** The authors would like to thanks the Fundação para a Ciência e Tecnologia (Lisboa, Portugal) under the frame of the Ciência 2007 program and FSE-FEDER (Project PTDC/QUI/71001/2006). R. Moreno-Tost thanks the Ministerio de Ciencia e Innovación (Spain) to support his Program Ramón y Cajal (RYC-2008-03387). It is acknowledged the Junta Andalucía (Spain).

## References

- Bruchez, M., Moronne, M., Gin, P., Weiss, S., Alivisatos, A.P.: Semiconductor nanocrystals as fluorescent biological labels. *Science* **281**, 2013–2016 (1998). doi:[10.1126/science.281.5385.2013](https://doi.org/10.1126/science.281.5385.2013)
- Michalet, X., Pinaud, F.F., Bentolila, L.A., Tsay, J.M., Doose, S., Li, J.J., Sundaresan, G., Wu, A.M., Gambhir, S., Weiss, S.: Quantum dots for live cells and in vivo imaging, diagnostics and beyond. *Science* **307**, 538–544 (2005). doi:[10.1126/science.1104274](https://doi.org/10.1126/science.1104274)
- Leitão, J.M.M., Gonçalves, H.M.R., Mendonça, C., Esteves da Silva, J.C.G.: Multiway chemometric decomposition of EEM of fluorescence of CdTe quantum dots obtained as function of pH. *Anal. Chim. Acta* **628**, 143–154 (2008). doi:[10.1016/j.aca.2008.09.020](https://doi.org/10.1016/j.aca.2008.09.020)
- Gonçalves, H.M.R., Mendonça, C., Esteves da Silva, J.C.G.: PARAFAC analysis of the quenching of EEM of fluorescence of glutathione capped CdTe quantum dots by Pb(II). *J. Fluoresc.* **19**, 141–149 (2009). doi:[10.1007/s10895-008-0395-1](https://doi.org/10.1007/s10895-008-0395-1)
- Braun, P.U., Osenar, P., Stupp, S.: Semiconducting superlattices templated by molecular assemblies. *Nature* **380**, 325–328 (1996). doi:[10.1038/380325a0](https://doi.org/10.1038/380325a0)
- Zhou, J., Yan, H., Zheng, Y., Wu, H.: Highly fluorescent poly(dimethylsiloxane) for on-chip temperature measurements. *Adv. Funct. Mater.* **19**, 324–329 (2009). doi:[10.1002/adfm.200800738](https://doi.org/10.1002/adfm.200800738)
- Li, D., Karne, R.B.: How nucleation affects the aggregation of nanoparticles. *J. Mater. Chem.* **17**, 2279–2782 (2007). doi:[10.1039/b700699c](https://doi.org/10.1039/b700699c)
- Jiménez-Jiménez, J., Rubio-Alonso, M., Quesada, D.E., Rodríguez-Castellón, E., Jiménez-López, A.: Synthesis and characterisation of acid mesoporous phosphate heterostructure (PPH) materials. *J. Mater. Chem.* **15**, 3466–3472 (2005). doi:[10.1039/b505973a](https://doi.org/10.1039/b505973a)
- Kresge, C.T., Leonowicz, M.E., Roth, W.J., Vartuli, J.C., Beck, J.C.: Ordered mesoporous molecular sieves synthesized by a liquid-crystal template mechanism. *Nature* **359**, 710–712 (1992). doi:[10.1038/359710a0](https://doi.org/10.1038/359710a0)
- Beck, J.S., Vartuli, J.C., Roth, W.J., Leonowicz, M.E., Kresge, C.T., Schmitt, K.D., Chu, C.T.W., Olson, O.H., Sheppard, E.W., McCullen, S.B., Higgins, J.B., Schlenker, J.L.: A new family of mesoporous molecular sieves prepared with liquid crystal templates. *J. Am. Chem. Soc.* **114**, 10834–10843 (1992). doi:[10.1021/ja00053a020](https://doi.org/10.1021/ja00053a020)
- Jiménez-Jiménez, J., Rubio-Alonso, M., Quesada, D.E., Rodríguez-Castellón, E., Jiménez-López, A.: Synthesis and characterization of mixed silica/zirconia and silica/titania porous phosphate heterostructures (PPH). *J. Phys. Solids* **67**, 1007–1010 (2006). doi:[10.1016/j.jpcs.2006.01.018](https://doi.org/10.1016/j.jpcs.2006.01.018)
- Zang, W.H., Shi, J.L., Wang, L.Z., Yan, D.S.: Preparation and characterization of ZnO Clusters inside mesoporous silica. *Chem. Mater.* **12**, 1408–1413 (2000). doi:[10.1021/cm990740a](https://doi.org/10.1021/cm990740a)
- Moreno-Tost, R., Olivera, M., Quesada, D.E., Jiménez-Jiménez, J., Jiménez-López, A., Rodríguez-Castellón, E.: Evaluation of Cu-PPHs as active catalysts for the SCR process to control NO<sub>x</sub> emissions from heavy duty diesel vehicles. *Chemosphere* **72**, 608–615 (2008). doi:[10.1016/j.chemosphere.2008.02.065](https://doi.org/10.1016/j.chemosphere.2008.02.065)
- Quesada, D.E., Ortiz, M.I.M., Jiménez-Jiménez, J., Rodríguez-Castellón, E., Jiménez-López, A.: Catalysts based on Ru/mesoporous phosphate heterostructures (PPH) for hydrotreating of aromatic hydrocarbons. *J. Mol. Catal. A Chem.* **255**, 41–48 (2006). doi:[10.1016/j.molcata.2006.03.059](https://doi.org/10.1016/j.molcata.2006.03.059)
- Lowndes, D.H., Fowlkes, J.D., Pedraza, A.J.: Early stages of pulsed-laser growth of silicon microcolumns and microcones in air and SF<sub>6</sub>. *Appl. Surf. Sci.* **154**, 647–658 (2000). doi:[10.1016/S0169-4332\(99\)00369-4](https://doi.org/10.1016/S0169-4332(99)00369-4)
- Chen, Y., Rosenzweig, Z.: Luminescent CdS quantum dots as selective ion probes. *Anal. Chem.* **74**, 5132–5138 (2002). doi:[10.1021/ac025825](https://doi.org/10.1021/ac025825)
- Jie, G., Liu, B., Pan, H., Zhu, J., Chen, H.: Cds nanocrystal-based electrochemiluminescence biosensor for the detection of low-density lipoprotein by increasing sensitivity with gold nanoparticle amplification. *Anal. Chem.* **79**, 5574–5581 (2007). doi:[10.1021/ac062357c](https://doi.org/10.1021/ac062357c)
- Cai, Z., Yang, H., Zhang, Y., Yan, X.: Preparation, characterization and evaluation of water-soluble L- cysteine-capped-CdS nanoparticles as fluorescence probe for detection of Hg(II) in aqueous solution. *Anal. Chim. Acta* **559**, 234–239 (2006). doi:[10.1016/j.aca.2005.11.061](https://doi.org/10.1016/j.aca.2005.11.061)
- Jiménez-Jiménez, J., Torres, P.M., Pastor, P.O., Rodríguez-Castellón, E., Jiménez-López, A.: Sol-gel synthesis of dodecyl-trimethylammonium-expanded zirconium phosphate and its application to the preparation of acidic porous oligomeric

- gallium(III)-exchanged materials. *Langmuir* **13**, 2857–2862 (1997). doi:[10.1021/la961073s](https://doi.org/10.1021/la961073s)
20. Li, Z., Du, Y., Zhang, Z., Pang, D.: Preparation and characterization of CdS quantum dots chitosan biocomposite. *React. Funct. Polym.* **55**, 35–43 (2003). doi:[10.1016/S1381-5148\(02\)00197-9](https://doi.org/10.1016/S1381-5148(02)00197-9)
21. Bhide, V.G., Salkalachen, S., Rastogi, A.C., Rao, C.N.R., Hegde, M.S.: Depth profile composition studies of thin film CdS:Cu<sub>2</sub>S solar cells using XPS. *J. Phys. D* **14**, 1647–1656 (1981). doi:[10.1088/0022-3727/14/9/012](https://doi.org/10.1088/0022-3727/14/9/012)
22. Gaarenstroom, S.W., Winograd, N.: Initial and final state effects in the ESCA spectra of cadmium and silver oxides. *J. Chem. Phys.* **67**, 3500–3506 (1977). doi:[10.1063/1.435347](https://doi.org/10.1063/1.435347)
23. Wang, C.Y., Mo, X., Zhou, Y., Zhu, Y.R., Liu, T., Chen, Z.Y.: A convenient ultraviolet irradiation technique for in situ synthesis of CdS nanocrystallites at room temperature. *J. Mater. Chem.* **10**, 607–608 (2000). doi:[10.1039/a908983g](https://doi.org/10.1039/a908983g)
24. Chen, S., Zhang, X., Zhang, Q., Tan, W.: Trioctylphosphine as both solvent and stabilizer to synthesize CdS nanorods. *Nano-scale Res. Lett.* **4**, 1159–1165 (2009). doi:[10.1007/s11671-009-9375-x](https://doi.org/10.1007/s11671-009-9375-x)
25. Unni, C., Philip, D., Gopchandran, K.G.: Studies on optical absorption and photoluminescence of thioglycerol-stabilized ZnS nanoparticles. *Opt. Mater.* (2009). doi:[10.1016/j.optmat.2009.06.019](https://doi.org/10.1016/j.optmat.2009.06.019)